JCTC Journal of Chemical Theory and Computation

Article

pubs.acs.org/JCTC

Ab Initio Parametrized Force Field for the Flexible Metal−Organic Framework MIL-53(Al)

L. Vanduyfhuys, T. Verstraelen,* M. Vandichel, M. Waroquier, and V. Van Speybroeck*

Center for Molecular Modeling (CMM), Ghent University (Member of the QCMM Ghent-Brussels Alliance Group), Technologiepark 903, 9052 Ghent, Belgium

Supporting Information

ABSTRACT: A force field is proposed for the flexible metal−organic framework MIL-53(Al), which is calibrated using density functional theory calculations on nonperiodic clusters. The force field has three main contributions: an electrostatic term based on atomic charges derived with a modified Hirshfeld-I method, a van der Waals (vdW) term with parameters taken from the MM3 model, and a valence force field whose parameters were estimated with a new methodology that uses the gradients and Hessian matrix elements retrieved from nonperiodic cluster calculations. The new force field predicts geometries and cell parameters that compare well with the experimental values both for the large and narrow pore phases. The energy profile along the breathing mode of the empty material reveals the existence of two minima, which confirms the intrinsic bistable behavior of the MIL-53. Even without the stimulus of external guest molecules, the material may transform from the large pore (lp) to the narrow pore (np) phase [Liu et al. *J. Am. Chem. Soc.* **2008**, *120*, 11813]. The relative stability of the two phases critically depends on the vdW parameters, and the MM3 dispersion interaction has the tendency to overstabilize the np phase.

1. INTRODUCTION

The discovery of metal−organic frameworks (MOFs)—a new class of nanoporous materials with exceptional physicochemical and mechanical properties—may be regarded as one of the major achievements within science in the past decade.[1−5] The chemistry and exploration of the properties of these materials is developing at an extraordinary pace with a huge number of research articles and reviews that appeared in the literature.[6−10] These materials consist of inorganic moieties connected by organic linkers and form a three-dimensional porous framework. There is an almost unlimited number of structures that may be proposed due to the chemical variety of both organic linkers and metal units at the nodal points. The resulting framework has very attractive features like high pore volumes with a diameter of up to 98 Å for IRMOF-74-XI[11] and a high Brunauer−Emmett−Teller surface area of up to 6240 m^2/gr for MOF-210.[12] It is especially this highly porous structure that makes these materials prime candidates for various industrial applications such as gas storage, purification or separation,[6,13−20] or liquid separation (e.g., fuels, xylenes).[21,22] The applications within catalysis are extensively investigated nowadays.[23−25] Excellent reviews on this topic appeared recently from the groups of Corma and Farrusseng.[26,27] Apart from these attractive features, some MOFs also exhibit intriguing flexible behavior, in which the pores can open or close reversibly upon external stimuli such as temperature,[28] electric or magnetic fields, mechanical pressure,[29] light,[30] or gas and liquid exposure.[15,31,32] Some of the typical examples showing this flexible or breathing behavior include MIL-88 and MIL-53, where cell parameters may vary drastically while the material retains its crystallinity.[33,34] The breathing is studied most extensively for the series of MIL-53 frameworks, which were originally synthesized and characterized by Férey and coworkers. A variety of compounds with chemical formula $M^{III}(OH)(BDC)$ (M^{III}= Al, Cr, Fe, Ga, Sc, and In; BDC^{2-} = terephthalate or 1,4-benzenedicarboxylate) have been synthesized.[31,33,35−39] This paper focuses on the MIL-53 framework with aluminum at the nodal points. MIL-53(Al) is built of long aluminum oxide chains connected to each other by terephthalic linkers, which results in a one-dimensional structure with a channel diameter of almost 10 Å, as schematically indicated by the green and blue tubes in Figure 1. This one-dimensional structure lies at the origin of the flexibility of some MOFs: the material can shrink or expand because the rigid linkers can hinge on the oxide chains. Most often the breathing behavior

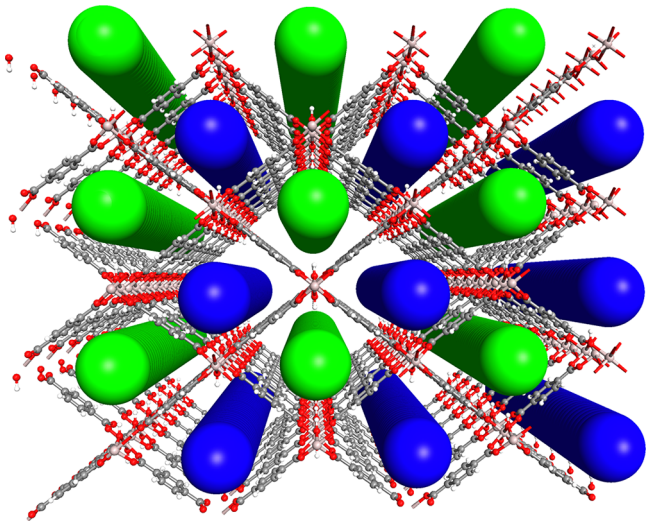

Figure 1. MIL-53(Al) and its 1D channels.

Received: February 29, 2012
Published: July 13, 2012

has been observed upon the adsorption of guest molecules.[15,31,32] However, Liu et al. recently reported the transition between two phases, i.e., a large pore (lp) and a narrow pore (np) without guest molecules but stimulated by temperature only.[28] The work of Liu et al. shows the intrinsic bistable behavior of the MIL-53(Al) host. Recently, Walker et al. were able to show the existence of two minima on the potential energy surface for the framework using density functional theory including an empirical dispersion term.[40] The np phase could only be retrieved by calculations including dispersive interactions.

DFT calculations are attractive due to their transferability to chemically very diverse systems, although they are also computationally very expensive and are not ideally suited to be used in molecular dynamics (MD) or Monte Carlo (MC) simulations, since such simulations typically run over longer length and time scales. MD and MC simulations are attractive to use in the study of adsorption and diffusion of guest molecules.[41−44] Apart from computational considerations, DFT is still hampered by the lack of dispersion effects in most of the frequently used functionals. The DFT-D method is the most commonly used approach nowadays to include these long-range interactions in which an empirical dispersion term is added to the DFT energy.[45,46] Another approach to address the dispersion interactions is the use of new density functionals that explicitly include dispersion interactions, such as M06-2X,[47,48] ωB97X-D,[49] vdW-DF,[50] and vdW-DF2.[51] Recently, the PBE-D2 method and vdW-DF, vdW-DF2, and some additional functionals have been tested for their performance in reproducing adsorption enhalpies of carbon dioxide in MOFs, and it was found that PBE-D2, vdW-DF, and vdW-DF2 compare extremely well with experimental results.[52]

An attractive approach used to perform atomistic simulations in which larger length and time scales are involved is the usage of a force field that neglects the detailed electronic structure of the MOF but approximates the potential energy surface (PES) as an analytical function of the nuclear coordinates. Such an approach is attractive as it allows one to perform a broad variety of simulations at a low computational cost. However, the approach is only successful if one possesses an accurate theoretical model for all the interactions that govern the behavior of the framework. Specifically stated, one needs a good mathematical model for the potential energy of the MOF framework as a function of its nuclear coordinates and cell parameters. Each analytical function of the force field corresponds to a certain internal degree of freedom and contains unknown parameters. These parameters can be recycled from existing force fields such as UFF,[53] DREIDING,[54] CVFF,[55] MM3,[56] and so on. For example, the group of Férey developed a force field for MIL-53(Cr) based on the CVFF and DREIDING force fields.[57] Another way to fix the unknown parameters would be to estimate them from a set of training data. One can either use experimental data such as geometries, vibrational modes, enthalpies of formation, or adsorption isotherms, or one can choose to use ab initio calculations performed on representative systems. Schmid and co-workers developed a force field for MOF-5 using DFT calculations on two representative clusters.[58] They also developed a genetic algorithm to derive force field parameters[59] and used it to derive a force field for the metal organic framework Cu-BTC.[60]

Another important aspect of a MOF force field is whether it treats the framework as rigid or flexible. In a simulation with a rigid framework, the atoms of the MOF are kept fixed while the guest molecules are allowed to move. Only the electrostatic and van der Waals interactions of the MOF with the guest molecules and the mutual interactions between the guest molecules are relevant. In a simulation with a flexible framework, the atoms of the framework are also allowed to move. The covalent interactions between the MOF atoms must also be addressed, and hence such a force field is called a covalent force field. Until recently, most of the MOF force-field simulations made use of a rigid framework. Schmid and co-workers pioneered the development of a force field for a MOF (MOF-5 in this case) in which the framework was flexible.[58] They showed that, for their force field, allowing the framework atoms to move during the simulation is crucial to correctly reproducing the diffusion coefficients of guest molecules in the MOF.[61] However, Ford et al. performed simular calculations with another force field[62] and found that the diffusion coefficient of benzene in MOF-5 is only mildly dependent on the framework flexibility.[63] It is clear that more research is needed to make a general conclusion on the influence of framework flexibility on the diffusion coefficients.

The purpose of this work is to derive a new force field for MIL-53(Al) from first principles and to develop new methodologies that facilitate the determination of the parameters. The force field has three main contributions: an electrostatic term, a van der Waals (vdW) term, and a conventional valence force field. The electrostatic part of the model is based on atomic point charges. Several methodologies used to assign atomic charges are tested and compared. The vdW term and the corresponding parameters are taken from the MM3 model of Allinger et al.[56] For the derivation of the valence parameters, i.e., the rest values and force constants, a new methodology is proposed. The force field is validated by comparing geometrical properties and cell parameters of the MIL-53(Al) framework with experimental data both for the lp and np phase. Additionally the force field is tested for its ability to reproduce the breathing phenomenon and more particularly to what extent the transition between the two phases can be predicted. This paper is a step toward the development of force fields that enable the predictive modeling of host−guest molecules in MOFs using a systematic methodology.

In the following two sections, we will outline the computational methods and the theoretical aspects of the force-field development. In the fourth section, the MIL-53(Al) force field is validated and applied to study the breathing effect. The fifth section summarizes our main conclusions. The Appendix discusses the technical details of the new calibration procedure for the valence force field.

2. COMPUTATIONAL DETAILS

Three kinds of calculations were performed in this work. Ab initio calculations on two nonperiodic clusters, ab initio calculations on the periodic MIL-53(Al), and force field calculations on the periodic MIL-53(Al).

The calculations on the nonperiodic clusters were performed as follows. The geometries of the isolated cluster models were fully optimized using Density Functional Theory (DFT) with the B3LYP[64−66] exchange correlation functional, which is an appropriate functional for the reproduction of molecular geometries.[67,68] Most of the atoms were described using a 6-311++G(d,p) basis set,[69−71] which includes diffuse functions for an improved description of the electron distribution in the oxygen anions. For the C−H atom pairs outside the core region

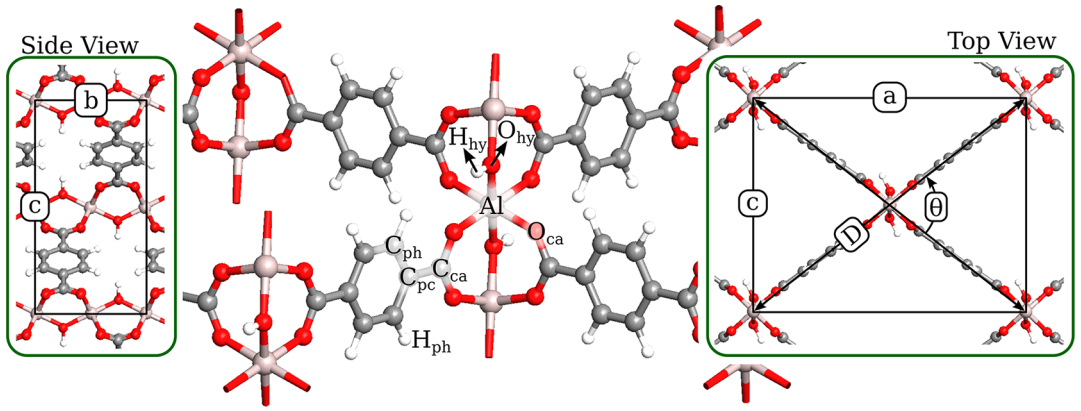

Figure 2. Definition of the force-field atom types in the periodic Mil-53(Al). The indentations visualize a side and top view together with the definition of the pricincipal axes of the unit cell, the diagonal D, and the interdiagonal angle θ.

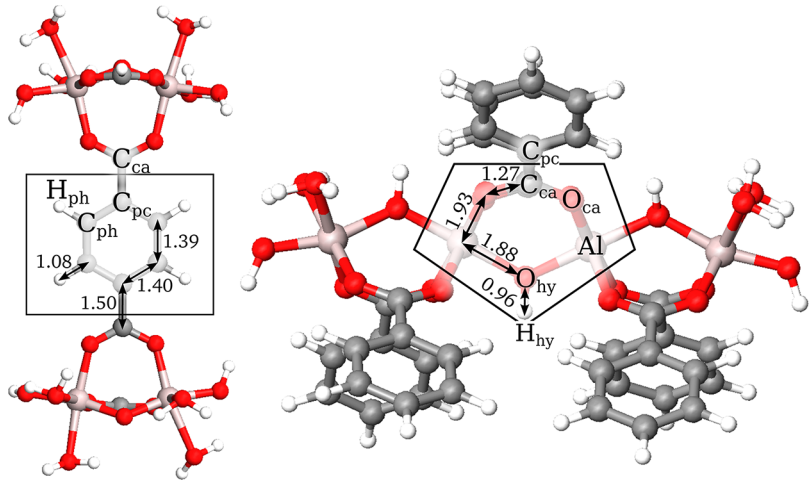

(a) linker (b) oxide

Figure 3. Nonperiodic clusters used to derive force field parameters for MIL-53. The core region of the cluster is indicated by a box, and some representative bond lengths are also given (in Ångströms). These were derived from the DFT calculations as specified in the Computational Details.

of the oxide cluster (explicit definition of the core region is given further in this paper), the computationally less expensive 6-31G(d,p) basis set[71,72] was used. The optimized clusters were confirmed to be true minima on the potential energy surface by performing a vibrational frequency analysis. These calculations also provide the Ab Initio (AI) forces and the Hessian matrix, i.e., the matrix with analytical second order derivatives of the energy toward the Cartesian coordinates, which are needed for the calibration of the force-field parameters. All cluster computations were carried out with Gaussian 09.[73]

In addition to these cluster calculations, we also performed periodic calculations on MIL-53(Al) with DFT, using the PBE[74,75] exchange correlation functional. A full geometry optimization of the periodic structure was performed using the GPAW[76−78] program with the projector-augmented wave method (PAW).[79,80] The pseudowave function in the PAW method was represented on a cubic real-space grid with a spacing of 0.2 Å. This wave function was used to derive atomic charges directly for the periodic structure. Furthermore, a DFT scan of the potential energy surface of the periodic structure was performed using the VASP[81−83] program. A Γ-point calculation was used with an energy cutoff of 600 eV, and the convergence criterion for the electronic self-consistent field (SCF) calculation was set to 10^{-6} eV. Furthermore, a Gaussian smearing[81] of 0.01 eV was applied. The reason we use different programs for the different periodic calculations is purely technical. We have chosen GPAW for the calculation of the periodic atomic charges because we found it more convenient to access the necessary quantities while we chose VASP for the periodic scan because it was found to be computationally more efficient to calculate a complete energy scan.

To validate the force field, several geometry optimizations were carried out with the new MIL-53(Al) force field. All these computations were performed with YAFF, a force field code developed in house. The simulations were performed using a supercell consisting of two unit cells aligned in the direction of the shortest cell vector. All derived properties are further given per unit cell. The electrostatic interactions were computed using an Ewald summation with a real space cutoff of 15 Å, α = 0.213, and a reciprocal space cutoff of 0.32 $Å^{-1}$.[84] The van der Waals interactions were also calculated with a smooth cutoff of 15 Å. A smooth cutoff for pairwise interactions indicates that the pairwise interaction energy is not simply truncated at the cutoff. Instead, we introduce a small transition region in which the energy smoothly evolves from the original expression to zero by means of a smoothing function, for which we used a cosine function. This smoothing avoids ill defined force components.

dx.doi.org/10.1021/ct300172m | J. Chem. Theory Comput. 2012, 8, 3217−3231

3. FORCE FIELD DEVELOPMENT

3.1. Choice of the Cluster Model Systems. In this work, Density Functional Theory (DFT) computations on two nonperiodic clusters are used to derive force-field parameters that can be applied to the periodic MIL-53(Al) system. There are two principal reasons to use cluster models: DFT computations on these clusters are computationally less demanding, and several well-established ab initio codes for isolated systems are available that can compute the Cartesian Hessian accurately. With the current computational resources, it is possible to extract the Cartesian Hessian matrix from periodic calculations, but such calculations come with a very high computational cost, especially when all normal modes need to have a positive frequency.[85] Therefore, preference was given to cluster models. However, one can only use these cluster models if the Hessian matrix elements are transferable to the periodic system. Therefore, one must carefully construct the isolated clusters such that they capture all the essential features of the periodic structure.

The structural topology of MIL-53 consists of tilted chains of $AlO_4(OH)_2$ octahedra, which are linked via carboxylate groups of the terephthalate ions (1,4-benzenedicarboxylate, BDC) creating a three-dimensional structure with an array of one-dimensional large pore channels shown in Figure 1. The chemical formula of the MIL-53(Al) is $Al(OH)(O_2C-C_6H_4-CO_2)$. A single unit cell is depicted in Figure 2, clearly showing the individual organic linkers connecting the metal-oxide chains. The nonperiodic clusters introduced in this study are shown in Figure 3. The first cluster contains a terephthalate linker at its center, while the second cluster is constructed around a segment of the metal-oxide chain. In order to select proper isolated cluster models, we considered the following guidelines:

1. The charge of the clusters should be as small as possible in order to avoid the introduction of electrostatic interactions that are unrealistic for the periodic structure.
2. The electronic structure of both clusters must be closed-shell systems, in line with the periodic MIL-53(Al) system.
3. The cluster should be large enough to capture all essential features of the periodic MOF structures. Not all force components and Hessian elements of the clusters are relevant for the periodic structure. Therefore, a core region was introduced as schematically depicted in Figure 3. Only force components of atoms in the core and Hessian elements of atom pairs of which at least one atom lies in the core are used for the further derivation of the force field. In this respect, the termination of the clusters must be well-separated from the core region (linker or oxide) of interest. In our cluster, the atoms belonging to the core regions are separated from terminating atoms by at least four bonds.
4. Each atom in the periodic MIL-53 structure must have an equivalent counterpart in the core region of one of the cluster models.

The proposed clusters in Figure 3, which were constructed using Zeobuilder,[86] fulfill these basic conditions. In the linker model (Figure 3a), the hydrogen atoms are removed from the bridging μ_2(OH) groups, and the oxide moieties are terminated by water molecules and hydroxyl groups to obtain a neutral closed-shell system.

The choice of a cluster which is representative for the inorganic building unit of MIL-53(Al) is less straightforward due to the occurrence of the one-dimensional chains formed by corner-sharing aluminum octahedra which are linked through μ_2(OH) bridging groups. Each aluminum center has two distinct types of Al−O linkages in the MIL-53 structure: four "equatorial" bonds to oxygens of the carboxylate ligands which are denoted by O_{ca} and two "axial" bonds along the chain direction which are denoted as O_{hy} (Figure 2). A first proposal for the inorganic cluster contained three aluminum atoms of the one-dimensional chain, as shown in Figure S1 of the Supporting Information. The oxide chain is terminated with water molecules and hydroxyl groups, while the linkers are terminated by replacing a carboxyl group by a hydrogen atom. We found that this first model is inadequate for a realistic description of the MIL-53 structure due to a poor description of the strong 1−5 electrostatic interactions between two O_{ca} atoms (separated by four covalent bonds) as indicated in Figure S1 in the Supporting Information. One of the atoms in this pairwise interaction is always close to the boundary of the cluster, leading to interactions that are not representative for the periodic system. Moreover the inorganic cluster with three aluminum atoms is not symmetric with respect to the central six-membered unit connecting two aluminum octahedra. At least four aluminum atoms are necessary to avoid these problems and to obtain a proper description of the periodic MIL-53 structure. The final cluster, shown in Figure 3b, has a total spin of zero and a total charge of +1 and fulfills other basic conditions as introduced before.

3.2. Force Field Energy Expression. The development of a force field (FF) consists of two steps: (i) the proposal of a suitable energy expression that depends on all internal coordinates and (ii) the estimation of the parameters figuring in the FF expression. The analytical expression for the force-field energy used in this work is given by

$$V^{\mathrm{ff}} = \underbrace{V_{\mathrm{bond}} + V_{\mathrm{bend}} + V_{\mathrm{torsion}}}_{V^{\mathrm{ff}}_{\mathrm{cov}}} + \underbrace{V_{\mathrm{el}} + V_{\mathrm{vdW}}}_{V^{\mathrm{ff}}_{\mathrm{noncov}}} \quad (1)$$

with

$$V_{\mathrm{bond}} = \sum_{i=1}^{N_r} \frac{1}{2} K_{r,i}(r_i - r_{i,0})^2 \quad (2)$$

$$V_{\mathrm{bend}} = \sum_{i=1}^{N_\theta} \frac{1}{2} K_{\theta,i}(\theta_i - \theta_{i,0})^2 \quad (3)$$

$$V_{\mathrm{torsion}} = \sum_{i=1}^{N_\phi} \frac{1}{2} K_{\phi,i}[1 - \cos(m_i \phi_i)] \quad (4)$$

$$V_{\mathrm{el}} = \frac{1}{2} \sum_{i \neq j}^{N_{\mathrm{at}}} \frac{q_i q_j}{4\pi\varepsilon_0 r_{ij}} \quad (5)$$

$$V_{\mathrm{vdW}} = \frac{1}{2} \sum_{i \neq j}^{N_{\mathrm{at}}} \varepsilon_{ij} \left[1.84 \times 10^5 \exp\left(-12 \frac{r_{ij}}{\sigma_{ij}} \right) - 2.25 \left(\frac{\sigma_{ij}}{r_{ij}} \right)^6 \right] \quad (6)$$

with N_r being the total number of stretch bonds, N_θ the total number of bending angles, N_ϕ the total number of torsions, and N_{at} the total number of atoms. This potential energy expression

consists of a part describing the *covalent* interactions (V^{ff}_{cov}), which are related to the presence of chemical bonds, and a part originating from *noncovalent* interactions (V^{ff}_{noncov}), which are governed by electrostatic and van der Waals interactions.

The harmonic model is not immediately applicable to the octahedral environment of aluminum. In particular, the four equatorial bonds with the oxygens of the carboxylate ligands have angular minima at 90° and 180°. Therefore, we used the improved Fourier-type angle-bending potential as proposed by Tafipolsky et al.[60,87,88] instead of the harmonic angle-bending term for the $O_{ca}-Al-O_{ca}$ angle:

$$V_{O_{ca}-Al-O_{ca}}(\theta) = \frac{K_\theta}{2}[1 + \cos(\theta)][1 + \cos(2\theta)] \quad (7)$$

Although the partitioning of energy terms into covalent and noncovalent parts seems trivial, it is merely an empirical and somewhat ambiguous convention. Using density functional theory, or any other electronic structure method, one cannot derive the covalent and noncovalent contributions separately. Electrostatic interactions are also present between bonded atoms, certainly when considering bonds with a strong ionic character. This is especially true for the bonds in the inorganic part of the MIL-53. Therefore, we choose to include electrostatic interactions between all pairs of atoms, as opposed to the conventional exclusion of certain pairs of atoms from the summation in eq 5 used in many other force fields. As such, the energy associated with chemical bonding will be determined by an electrostatic contribution and a residual covalent part.

The electrostatic interaction V_{el} is modeled by using constant atomic charges, and the sum runs over all atom pairs excluding self-interactions. More information on the determination of the atomic charges is given in section 3.3.

The van der Waals part of the noncovalent energy is modeled by the MM3-vdW[56] term in eq 6; the numbers 1.84×10^5 and 2.25 originate from the work of Allinger and co-workers.[56] σ_{ij} denotes the sum of the van der Waals radii: $\sigma_I + \sigma_j$. The energy parameter, ε_{ij}, is derived from atomic parameters by taking the geometric mean, i.e., $\varepsilon_{ij} = (\varepsilon_i\varepsilon_j)^{1/2}$. In this equation, the summation in the vdW interactions runs over all atom pairs excluding pairs involved in bonds (so-called 1−2 pairs) and valence angles (1−3 pairs). Without such exclusion rules, one would get strongly overestimated repulsion terms that would distort bond lengths and valence angles.

To limit the number of independent parameters in the energy expression, force-field atom types are introduced as shown in Figure 2. For the covalent interactions, unique parameters are associated with each pair (for bonds), triplet (for angles), or quadruplet (for torsions) of force-field atom types. Each atom type is associated with a unique set of atomic vdW parameters and an atomic charge.

3.3. Atomic Charges for the Electrostatic Interactions.

Atomic charges are a key ingredient to modeling the electrostatic interactions and are also convenient properties to understand chemical interactions. However, they are nontrivial to define from a quantum-mechanical perspective: many different theoretical schemes have been proposed in the literature over the past 60 years to derive Atom-in-Molecule (AIM) charges, which do not necessarily lead to consistent results. Some of the more popular schemes are Mulliken population analysis,[89] natural population analysis,[90] (iterative) Hirshfeld partitioning,[91,92] ESP-fitted charges,[93−95] and QTAIM charges.[96]

For the development of force-field models, one often relies on ESP-fitted charges because they reproduce the electrostatic potential surrounding the molecule.[97,98] Ramsahye et al.[99] calculated ESP-fitted charges for MIL-53(Al). Especially the RESP[95] method is popular in limiting the statistical deficiencies of ESP-fitted charges. Despite the restraining techniques used in the RESP scheme, RESP charges are still very sensitive to conformational changes.[100] One can also reduce the rank deficiency[101] of ESP-fitted charges by using a limited set of bond-charge-increment (BCI)[102] parameters associated with certain pairs of atom types.[97]

Recently, the Hirshfeld-I[92] partitioning scheme was proposed, which relies on a partitioning of the electron density. Several studies showed that this new scheme results in charges that reproduce the electrostatic potential with nearly the same accuracy as ESP-fitted charges for organic molecules.[103] Moreover, the Hirshfeld-I charges are very robust with respect to conformational changes, which is clearly an advantage over the ESP-fitted charges,[100,104] and only show a weak dependence on the basis set used in the quantum mechanical calculations.[92] Nevertheless, also the Hirshfeld-I method has its deficiencies. A recent study of charge equilibration models for silicates revealed that the Hirshfeld-I method overestimates (in absolute value) the charges of systems with a strong ionic character. For example, this error leads to systematically overestimated dipole moments for a large set of silica clusters.[105] Therefore, we suggest herein a modified version of the method, hereafter called *valence Hirshfeld-I* (VHI), where the core electrons are assigned to their native atoms and only the valence electrons are partitioned with the Hirshfeld-I scheme.

In what follows, MIL-53(Al) charges are derived from the isolated cluster computations and from the periodic DFT calculation using GPAW (see Computational Details). The charges derived from the periodic system serve as a validation of the results obtained with the cluster computations. For the derivation of the valence parameters in the following section, we need the charges on all atoms in the cluster models to subtract the electrostatic interactions from the DFT training data.

Three sets of charges are derived from the cluster computations: Hirshfeld-I charges (HI), valence Hirshfeld-I charges (VHI), and ESP-fitted charges (ESP); the hirshfeld-based charges are included in Tables S1−S3 of the Supporting Information. The ESP cost function is taken from ref 105. To derive charges for the periodic system from these data, one cannot simply transfer the charges obtained for the core regions of both linker and oxide cluster to the periodic system, because this procedure would not result in a neutral MIL-53(Al) framework. To circumvent this problem, we introduce bond-charge-increments (BCIs),[102] p_{ij}, which are defined as charge tranfers along neighboring atoms and which are related to atomic charges, q_i, as follows:

$$q_i = \sum_j{}' p_{ij} + q_i^0 \quad \forall\ i \text{ with } p_{ij} = -p_{ji} \quad (8)$$

where the sum is limited to atoms j that are bonded to atom i. The precharge q_i^0 is introduced to treat systems that are not neutral.[97] The introduction of this precharge is only needed for the oxide cluster, where all precharges are set equal to the total charge divided by the number of atoms.[105] The procedure to transfer the charges from the cluster calculations to the periodic structure is as follows: first, the HI and VHI charges are transformed to BCIs associated with pairs of atom types (see

Figure 2), by inverting eq 8 using a least-squares method. Second, the fitted BCIs of the core of each cluster are transferred to the periodic system. This uniquely defines all BCIs of the periodic system, except for $C_{ca}-C_{pc}$ pairs because it crosses the core boundary in both clusters. However, the BCIs deduced from both clusters are very similar and thus it does not make much difference which one we use in the periodic system. We have chosen the one from the oxide cluster. One should avoid to transform ESP-fitted charges a posteriori to BCIs due to the statistical noise on the charges. Instead, BCI parameters were fitted directly to ESP grid data.[97] The atomic charges for the MIL-53(Al) framework in its large pore form, obtained by applying the BCIs derived from the clusters, are shown in the first three columns of Table 1.

Table 1. Atomic Charges for the MIL-53(Al) Framework in Its Large Pore Form (in e) Calculated Using Different Methods[a]

	cluster-based			periodic	
atom type	HI	VHI	ESP	AHI	AESP
Al	2.939	2.078	2.002	2.058	2.075
C_{ca}	0.996	0.885	0.899	0.839	0.664
C_{pc}	−0.154	−0.111	−0.041	−0.106	0.067
C_{ph}	−0.071	−0.091	−0.145	−0.099	−0.180
H_{hy}	0.566	0.515	0.418	0.508	0.422
H_{ph}	0.124	0.127	0.148	0.133	0.161
O_{ca}	−0.879	−0.740	−0.810	−0.699	−0.702
O_{hy}	−1.882	−1.322	−0.906	−1.368	−1.081

[a]HI refers to the Hirshfeld-I method, VHI to the valence Hirshfeld-I method, and ESP stands for ESP-fitted charges. AHI are Hirshfeld-I charges obtained by partitioning the auxiliary density, and AESP stands for charges derived from the electrostatic potential due to the auxiliary density. The atom types are depicted in Figure 2.

Charges were also derived from periodic calculations on the lp variant of the Mil-53(Al) using the GPAW[76−78] method to validate the accuracy of the cluster-based charges. In the projector augmented wave (PAW) scheme,[79,80] the auxiliary density only accounts for a fraction of the total electron density, which roughly corresponds to the density of the valence electrons. This auxiliary density was partitioned using the Hirshfeld-I scheme (AHI), and the electrostatic potential due to the auxiliary density was used to fit ESP-charges (AESP). Both types of charges were corrected with the atomic compensation charges, which account for the contributions that are missing in the auxiliary density of the PAW scheme. The results are given in the last two columns of Table 1.

The charges for Al and O_{hy} obtained with the HI method deviate significantly from the other methods, which agrees with earlier work where similar deviations were observed for charges in silicates.[105] The four other schemes lead to much more consistent results. The good correspondence between the periodic and cluster results confirms the robustness of the transformation between atomic charges and bond-charge increments. We already mentioned that we need charges for all atoms in the clusters; hence we need to choose a cluster-based scheme. We choose to proceed with the VHI charges because the differences between ESP and AESP charges are larger than the differences between VHI and AHI, indicating that the ESP-based charges are not as robust.

3.4. van der Waals Parameters. The van der Waals (vdW) parameters are taken from the MM3 force field of Allinger et al.[56,106] and are given in Table 2. The accuracy of the repulsion between apolar hydrogen atoms is problematic in the MM3 model and may be improved by displacing the interaction site for the van der Waals interaction of such hydrogen atoms along the R−H bond.[56] However, comparison of the force-field interaction energy, consisting of nonbonded contributions only, of two benzene molecules with DFT revealed that the repulsion between hydrogen atoms of nearby linkers is acceptable when the MM3 vdW parameters are used without any correction. Hence the displacement of the van der Waals interaction site of the aromatic hydrogen atoms was not implemented. Such corrections may become relevant when studying the adsorption of guest molecules in the MIL-53 framework. Therefore, an extended recalibration of the repulsion and dispersion interactions will be considered in future work. In this paper, we focus on testing new methods to derive electrostatic and valence parameters, which will be discussed in the following subsections.

Table 2. MM3 van der Waals Parameters[a]

atom type	σ_i [Å]	ε_i [kJ mol^{-1}]	MM3 atom type
Al	2.36	0.485	aluminum (-)
C_{ca}	1.94	0.234	sp^2 carbon (2)
C_{pc}	1.94	0.234	sp^2 carbon (2)
C_{ph}	1.94	0.234	sp^2 carbon (2)
H_{hy}	1.60	0.067	alcohol hydrogen (21)
H_{ph}	1.62	0.084	aromatic hydrogen (5)
O_{ca}	1.82	0.247	oxygen in carboxyl anion(47)
O_{hy}	1.82	0.247	alcohol oxygen (75)

[a]The aluminum parameters are taken from ref 106. All other parameters are taken from the mm3.prm file from the TINKER[107] package, which is based on ref 56. The number between parentheses is the atom type number from the mm3.prm file.

3.5. Covalent Parameters. As discussed above, the electrostatic interactions in this work are treated differently compared to most conventional force-field models: pairwise electrostatic interactions are included between all atom pairs without applying any scaling or exclusion rules. This approach can be well motivated in our case since the bonds in the oxide moiety of the system have a strong ionic character. In the total force field expression, both covalent and electrostatic terms are present and the sum of both needs to be described accurately. This implies that the covalent terms must be fitted to reproduce the differences between the ab initio training data and the electrostatic term (V_{el}). This mainly affects the oxide parameters in the model, where the electrostatic term is strongly attractive for bonded atoms (such as the pair $Al-O_{ca}$) and the corresponding covalent terms will be repulsive at small interatomic distances. There is no need to subtract the van der Waals terms from the DFT computations because (i) the vdW contribution is excluded for 1−2 and 1−3 pairs and (ii) the long-range dispersion effects are absent in DFT reference data due to the known limitations of the B3LYP functional.[45]

Several schemes exist to estimate the covalent parameters from training data generated from first principles. We can group these schemes according to the training data that are used for the fitting procedure. A first class uses only information directly related to the potential energy surface (e.g., gradient, Hessian, ...),[108−112] and a second class also uses information from derived quantities (e.g., geometry, normal modes, ...)[59,113] or even statistical observables.[114−116] It is conceptually attractive

to calibrate force-field parameters to reproduce the (derived) observables of interest, but such schemes are computationally demanding and provide little insight into the topology of the parameter space. The deduction of the parameters is not straightforward: one has to perform multiple force field simulations at each iteration of the parameter calibration, and it is hardly possible to compute analytical derivatives of the cost function toward the force field parameters. In that case, one can only use Monte Carlo methods or genetic algorithms to optimize the parameters.[59]

In this work, the parameters are calibrated using the gradients and Hessian matrix elements from the ab initio calculations. Only gradients that belong to atoms of the core region of the clusters and Hessian matrix elements for which at least one of the involved atoms belong to the core region for the clusters are used. Basically, the valence parameters are deduced by solving the following sets of equations

$$G^{\mathrm{ai}} = G^{\mathrm{ff}}_{\mathrm{cov}} + G^{\mathrm{ff}}_{\mathrm{el}} \tag{9}$$

$$H^{\mathrm{ai}} = H^{\mathrm{ff}}_{\mathrm{cov}} + H^{\mathrm{ff}}_{\mathrm{el}} \tag{10}$$

where G^{ai} is the ab initio energy gradient corresponding to the derivative of the ab initio energy toward the Cartesian coordinates. $G^{\mathrm{ff}}_{\mathrm{cov}}$ and $G^{\mathrm{ff}}_{\mathrm{el}}$ are Cartesian derivatives of the force-field energy contributions $V^{\mathrm{ff}}_{\mathrm{cov}}$ and V_{el} of eq 1, respectively. H^{ai} is the ab initio Hessian, containing the second derivatives of the ab initio energy toward the Cartesian coordinates, and similar definitions hold for $H^{\mathrm{ff}}_{\mathrm{cov}}$ and $H^{\mathrm{ff}}_{\mathrm{el}}$. Such equations can be solved using a least-squares technique to obtain the optimal parameters using the Levenberg−Marquardt algorithm. Two crucial modifications of these equations were needed, which will be briefly discussed below. More information on the procedure may be found in the Appendix.

Both modifications mainly affect the gradient equations (eq 9). Without any modifications, the gradient equations are compatible with the force-matching method that is often used in conjunction with ab initio molecular dynamics simulations.[108] Since both isolated clusters are optimized at the DFT level, the left-hand side of these equations is zero ($G^{\mathrm{ai}} = 0$).

In the hypothetical case that parameters are found such that the force-field gradient also becomes zero for both clusters, the force field would exactly reproduce the ab initio geometries. However, in reality the gradient equations are only solved approximately, and the errors on the force-field gradient will lead to errors in the force-field geometry. Because this error is distributed equally over all components of the Cartesian gradient, the error on the geometry will be especially large (or small) along shallow (or steep) modes of the potential energy surface. Since our primary goal is the construction of a force-field that correctly reproduces geometries, we have introduced additional weight factors in the gradient equations which depend on the Hessian and which give higher weights to the gradient along shallow modes. This ensures that the PES is more accurately determined along shallow modes of the surface. More details about the mathematical derivation can be found in the Appendix.

The second adjustment is an additional set of equations to address the strong correlations between the rest parameters, i.e., the parameters $r_{i,0}$ and $\theta_{i,0}$ in eqs 2 and 3. A well-known difficulty with force field calibrations is the redundancy of the internal coordinates.[111,117] The number of internal coordinates usually largely exceeds the number of Cartesian degrees of freedom. Due to this redundancy, certain linear combinations of internal coordinates do not have a corresponding Cartesian degree of freedom. Consider for example the angles in a planar six-membered ring. It is not possible to increase all six angles equally, and hence an angular force that tries to increase all angles would cancel out when transformed to Cartesian coordinates. This is a direct result from the fact that there are only five independent angles, while the sixth is constrained by the geometrical requirement that the sum of the angles is 720°. The gradient equations above (or any of its variants) are not sensitive to such internal strains, i.e., combinations of internal forces that cancel each other out when transformed to Cartesian coordinates, because they only consider the Cartesian gradient. In case of the six-membered ring, the gradient equations would not be able to fix the rest value of the angle bending term. The additional equations introduced in this work require that all of the internal strains, i.e., linear combinations of derivatives of covalent energy terms that do not contribute to the Cartesian forces, are equal to zero. More details on how this is precisely done are given in the Appendix.

In order to find the optimal covalent parameters, a cost function is constructed that takes the errors on the three sets of equations discussed above into account: (i) transformed gradient equations, (ii) Hessian equations, and (iii) internal strain equations. The parameters that minimize this cost function are given in Table 3 and will be used in the covalent contributions of the force field. The optimization of the covalent parameters was done using the in-house developed software packages FFit2 and MolMod.[118] It is immediately clear that the rest parameters of the bonds in the oxide chain are larger than the typical equilibrium value of the corresponding internal coordinates (see Figure 3). These are ionic bonds that have a significant attractive electrostatic contribution due to the large and opposite charges on the atoms involved. At the equilibrium bond length, this is compensated by a repulsive covalent bond term. Similarly, the rest angles of the Al−O_{ca}−C_{ca} and Al−O_{hy}−Al bends are lower than the equilibrium values due to the repulsion of, respectively, Al−C_{ca} and Al−Al. A more prominent illustration can be found in the force constant of the O_{ca}−Al−O_{ca} bend, which is equal to zero. Apparently, the electrostatic repulsion of the O_{ca} atoms can fully account for the interaction energy of the angle bending.

3.6. Ab Initio Scan of the Periodic Cell. Table 3 reveals that the force constants of the dihedral angles Al−O_{ca}−C_{ca}−C_{pc} (K_c) and Al−O_{ca}−C_{ca}−O_{ca} (K_o) are relatively small. This is an indication that these torsions may show anharmonic behavior and hence that the proposed energy term (eq 4) is not the most suitable term to describe these torsional motions. Furthermore, the force constants (K_c and K_o) are prone to statistical noise: small deviations on the weights in the cost function (see Appendix) result in significant deviations on these force constants. In order to investigate the validity of the harmonic terms for these dihedral motions, we performed additional periodic DFT computations with VASP (see Computational Details) from which also K_c and K_o are deduced.

Figure 4 gives a visual representation of the dihedral motions of interest. The dihedral angle Al−O_{ca}−C_{ca}−C_{pc} determines the rotation of a linker about the two O_{ca}−O_{ca} axes of the carboxyl groups in the linkers (φ_1). This rotation enables shrinkage or expansion of the entire unit cell. The dihedral angle Al−O_{ca}−C_{ca}−O_{ca} controls the tilting of the plane of the linker (illustrated by the rectangular shaded area) around the C_{ca}−C_{pc}−C_{pc}−C_{ca} axis (φ_2). This tilting also induces an opposite rotation of two neighboring Al(O_{ca})$_4$ planes (illustrated by the

Table 3. Parameters of the Covalent Contributions to the Force Field[a]

bonds	K [kJ mol^{-1} Å^{-2}]	r_0 [Å]
Al−O_{ca}	1079	2.151
Al−O_{hy}	1738	2.137
C_{ca}−O_{ca}	5466	1.337
C_{ca}−C_{pc}	2580	1.508
C_{ph}−C_{pc}	2897	1.398
C_{ph}−H_{ph}	3420	1.086
C_{ph}−C_{ph}	3413	1.386
O_{hy}−H_{hy}	7030	1.046
bends	K [kJ mol^{-1} rad^{-2}]	θ_0 [deg]
Al−O_{ca}−C_{ca}	58	87.7
Al−O_{hy}−Al	173	73.5
Al−O_{hy}−H_{hy}	104	85.0
O_{ca}−Al−O_{ca}	0	
O_{ca}−Al−O_{hy}	121	91.1
O_{ca}−C_{ca}−O_{ca}	672	122.9
O_{ca}−C_{ca}−C_{pc}	136	123.8
O_{hy}−Al−O_{hy}	0	
C_{ca}−C_{pc}−C_{ph}	678	120.7
C_{pc}−C_{ph}−C_{ph}	448	121.6
C_{pc}−C_{ph}−H_{ph}	297	121.4
C_{ph}−C_{pc}−C_{ph}	345	118.4
C_{ph}−C_{ph}−H_{ph}	351	122.0
dihedrals	K [kJ mol^{-1}]	
Al−O_{ca}−C_{ca}−C_{pc}	3 (14)[a]	
Al−O_{ca}−C_{ca}−O_{ca}	14 (11)[a]	
C_{pc}−C_{ph}−C_{ph}−H_{ph}	36	
C_{pc}−C_{ph}−C_{ph}−C_{pc}	41	
C_{ph}−C_{ph}−C_{pc}−C_{ph}	32	
C_{ph}−C_{ph}−C_{pc}−C_{ca}	58	
C_{ph}−C_{pc}−C_{ca}−O_{ca}	23	
H_{ph}−C_{ph}−C_{ph}−H_{ph}	23	
H_{ph}−C_{ph}−C_{pc}−C_{ph}	27	
H_{ph}−C_{ph}−C_{pc}−C_{ca}	29	

[a]The values between brackets are determined using the ab initio scan (see section 3.6).

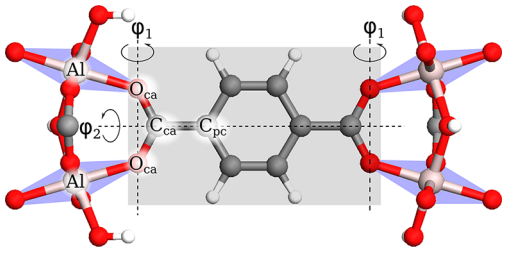

Figure 4. Illustration of the dihedral motions. The dashed lines indicate rotation axes. The rectangular shaded area highlights all the atoms that take part in the rotations, and the blue parallelograms show the Al(O_{ca})$_4$ planes.

blue parallelograms) about the Al−Al axis. Both the linker rotation and tilting are strongly influenced by the constraints imposed by the periodic structure of the MOF. Therefore, it may be anticipated that periodic calculations are necessary to get a good estimate of the force constants of these dihedral motions. This was investigated by performing a scan in terms of the interdiagonal angle θ, which is defined in Figure 2. To limit the computational complexity of the scan, we generated a trajectory using the force field (instead of using an ab initio trajectory) and calculated the DFT energy for every frame in the trajectory. Constrained geometry optimizations, using the initial parameters of the force field as tabulated in Table 3, were performed, in which the interdiagonal angle θ was varied from 30° to 90° with a step of 1°. The interdiagonal angle θ and the diagonal length D are indicated in Figure 2 and are defined as

$$D = \sqrt{a^2 + c^2} \tag{11}$$

$$\theta = 2\arctan\left(\frac{a}{c}\right) \tag{12}$$

It is the intention to estimate new values for the two dihedral force constants K_c and K_o that reproduce the DFT energy along the trajectory as well as possible. For that purpose, we decompose the force field energy into three parts:

$$V_{dft} = V_{res} + V_{vdw} + V_{dih} \tag{13}$$

with

$$V_{dih} = K_c V_c + K_o V_o \tag{14}$$

V_{dih} contains the two contributions to the dihedral force-field energy that relate to the parameters K_c and K_o which need to be determined. V_c and V_o represent these two contributions with the value of their respective force constant set at 1 kJ mol^{-1}. V_{vdw} is the MM3-vdW contribution to the force-field energy, and V_{res} contains all of the remaining contributions (bonds, bends, remaining dihedrals, and electrostatic interactions) of V^{ff}. By investigating all contributions to the force-field energy, we notice that dispersion interactions and Pauli repulsion both have a large influence on the energy profile. However, dispersion is neglected in most DFT functionals. Recently, new functionals were suggested that include dispersion, and additionally the popular DFT-D method is regularly used in which an empirical van der Waals correction is added to the DFT energy.[45−47,119] As it is unclear at this point to what extent the MM3-vdW contribution performs well at reproducing the dispersion interaction of these new DFT approaches, we performed the scan with regular PBE but drop the dispersion contribution from the FF energy during the scan. This will enhance the Pauli repulsion contribution in the force field because at short internuclear distances, dispersion compensates Pauli repulsion. To correct for this, we uniformly scale the Pauli interactions, V_{pauli}, with a factor ζ which will be determined hereafter before finding the most optimal values for K_c and K_o.

The result from the energy scan and the various energy contributions are shown in Figure 5. The torsional energies V_c and V_o are more or less constant in a small range of interdiagonal angles (30−36°), giving rise to a constant contribution $K_cV_c + K_oV_o = V_{dih}$ (green curve in Figure 5). Hence, we can use this tail to estimate ζ by solving

$$\Delta V_{dft} = \Delta V_{res} + \zeta \Delta V_{pauli} \tag{15}$$

for all interdiagonal angles in the range of 30−36° using a least-squares technique. This leads to a scaling factor ζ = 0.65. In a second step, we can use this ζ and solve eq 13 (in which all contributions are expressed relative to θ = 90°) in the least-squares sense over the entire range of the interdiagonal angle to estimate the force constants K_c and K_o. This procedure results in the following values for K_c and K_o:

$$K_c = 13.6 \text{ kJ mol}^{-1} \tag{16}$$

$$K_o = 11.1 \text{ kJ mol}^{-1} \tag{17}$$

dx.doi.org/10.1021/ct300172m | J. Chem. Theory Comput. 2012, 8, 3217−3231

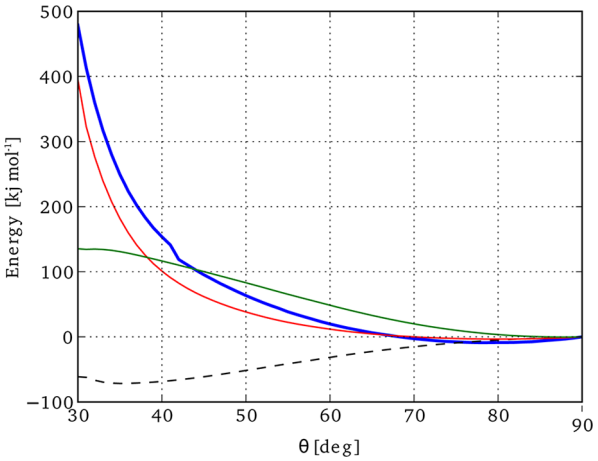

Figure 5. Relevant energies of the periodic ab initio scan: total DFT energy V_{dft} (bold blue), force-field residual energy V_{res} (dashed black), ζ-scaled Pauli energy ζV_{pauli} (red), fitted dihedral energy V_{dih} (green). All energies are expressed relative to $\theta = 90°$.

Figure 5 shows the results of the fit using these new values for K_c and K_o. Using these force constants, we calculated the root-mean-square-deviation Δ between the DFT energy and the total force-field energy and found $\Delta = 0.94$ kJ mol^{-1}. This small deviation indicates that the functional form proposed in eq 4 is a good choice, and there is no need for additional anharmonic contributions. Comparing the new force constants with their original values from Table 3, we see that there is a large difference, especially for the dihedral Al−O_{ca}−C_{ca}−C_{pc}, indicating that the equilibrium forces and Hessian of the two clusters do not contain enough information about these dihedral motions. The scan of the periodic unit cell is indeed mandatory in order to describe the dihedrals accurately. The new force constants are indicated in Table 3. From now on, we will use these values in the force-field simulations. In the remainder of the paper, the van der Waals parameters are reset to their former MM3 values, including Pauli and dispersion. No scaling is applied anymore, because the scaling procedure was only necessary to compensate for the neglect of dispersion interactions in this section.

4. FORCE FIELD APPLICATIONS AND VALIDATION

4.1. Geometry Optimization. A first validation of the force field is the correct prediction of the geometry in both the np and lp form. The cell parameters and the fractional coordinates of the periodic structure were optimized using the new force field. The final geometry obtained in lp is shown in Figure 6. Some essential internal coordinates from the core region of both isolated clusters are compared with their force-field counterparts in the optimized periodic structure (see Table 4). The table also shows a force-field simulation in which MM3-vdW interactions are switched off (see column *ForceField(no-vdW)*). Such a comparative study can be very instructive to explore the main differences in the optimized geometry by taking into account vdW interactions or not. Since only the covalent and electrostatic interactions of the FF are fitted to the DFT calculations—and not the vdW interactions—we could expect that the FF-no-vdW simulation will generate geometrical parameters close to the DFT values. This is indeed the case. The largest discrepancies are noticed in the predictions of the bond Al−O_{hy} and the bending angles Al−O_{ca}−C_{ca} and Al−O_{hy}−Al, which are severely underestimated.

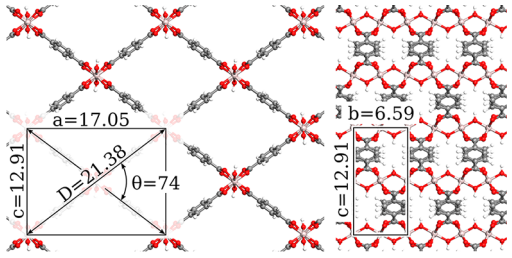

Figure 6. Top and side view of the unit cell in the lp phase after a geometry optimization using the force field (with MM3 vdW). The unit cell and its dimensions are also shown; lengths are in angstroms and angles in degrees.

Table 4. Some Key Bond Distances and Angles Obtained in the Force Field and DFT Optimized Cluster Geometries[a]

	force field		
	MM3-vdW	*no-vdW*	DFT-cluster
	bond lengths [Å]		
Al−O_{ca}	1.932	1.927	1.927
Al−O_{hy}	1.878	1.861	1.882
O_{ca}−C_{ca}	1.267	1.266	1.268
C_{ca}−C_{pc}	1.503	1.489	1.496
C_{ph}−C_{ph}	1.391	1.387	1.389
C_{ph}−C_{pc}	1.409	1.398	1.399
	bending angles [deg]		
Al−O_{ca}−C_{ca}	132.0	127.8	134.5
Al−O_{hy}−Al	122.7	121.0	126.4
O_{ca}−Al−O_{hy}	90.0	90.0	89.7
O_{ca}−Al−O_{ca}	90.0	90.0	90.0
O_{ca}−C_{ca}−O_{ca}	123.5	124.1	124.5

[a]The force-field internal coordinates are given both for a force-field optimization with MM3-vdW interactions switched on (*MM3-vdW*) and with vdW interactions switched off (*no-vdW*).

This is not completely surprising since the Pauli repulsion in the metal oxide chain is not involved in the FF-no-vdW results. The three geometrical variables under consideration are much better reproduced in the MM3-vdW simulations, and this confirms our expectations. In general, the agreement is very satisfactory, and this provides good evidence that the covalent and electrostatic interactions succeed in reproducing the ab initio calculations.

In the next step, we compared the simulated cell dimensions of both lp and np phases with the experimental values of the empty host at 77 K from ref 28 (see Table 5). The interdiagonal angle θ and diagonal length D defined in Figure 2 are also tabulated. For the lp, the agreement between simulation and experiment is very good: the simulation predicts an orthorhombic shape, in agreement with the experiment, and the deviation between simulation and experiment on the interdiagonal angle θ and the diagonal length D is around 1%. Furthermore, the force field also performs reasonably well at reproducing the unit cell of the np phase; especially the reproduction of the interdiagonal angle θ is very good. There is however a rather large deviation in the diagonal length (6.3%), and at this point, we do not have a clear explanation for this discrepancy. The force field also predicts a nonorthorhombic shape of the unit cell, in agreement with the experiment, albeit a diclinic shape with smaller angles instead of a monoclinic shape. However, overall we can conclude that the force field succeeds in predicting the geometries of both lp and np phases.

dx.doi.org/10.1021/ct300172m | J. Chem. Theory Comput. 2012, 8, 3217−3231

Table 5. Comparison of Cell Parameters[a]

	experimental (77 K)		simulated	
	lp	np	lp	np
a [Å]	16.913	20.824	17.046	19.565
b [Å]	6.624	6.607	6.593	6.527
c [Å]	12.671	6.871	12.905	6.245
α [deg]	90.000	90.000	90.000	87.891
β [deg]	90.000	90.000	90.000	89.434
γ [deg]	90.000	113.949	90.632	97.150
D [Å]	21.133	21.928	21.380	20.537
θ [deg]	73.680	36.522	74.254	35.407

[a]The experimental values of the empty host (at 77 K) are taken from ref 28. Simulated cell parameters are obtained by minimizing the force-field energy of the MIL-53(Al) structure.

This is especially promising since the information on the np phase was only used for fine-tuning two dihedral force constants. The force field was additionally tested for its sensitivity with respect to some crucial parameters. We selected K_c and K_o, as these are the two dihedral force constants which are crucial to describing the structural transition of the material. The results may be found in the Supporting Information. We found that the interdiagonal angle in the narrow pore and the diagonal length in both phases are insensitive to changes in these force constants, while the interdiagonal angle in the large pore is more sensitive.

4.2. Energy Profile during Breathing. MIL-53(Al) is the most studied example of a flexible MOF with its specific breathing behavior. Upon adsorption of guest molecules, the framework can switch reversibly between a large pore (lp) and a narrow pore (np) form.[15,31,32] In the case of H_2O as an adsorbent, the observed structural transition is mainly due to the hydrogen bond interaction between water and the oxygens of the MOF carboxylates.[31] However, there is experimental evidence that these structural transitions also take place in the absence of guest molecules, indicating that the framework is intrinsically bistable.[28] The energy barrier between the two forms is very low, allowing for thermally induced transitions between the two forms. The intrinsic bistability of MIL-53(Al) has already been investigated in the literature by Walker et al.[40] based on DFT-D computations. These calculations showed that the np form is more stable than the lp form with values ranging from 34 to 42 kJ mol^{-1} per unit cell. These energy differences include a large fraction of dispersion interaction (ranging from 150 to 184 kJ mol^{-1} per unit cell). The authors conclude that dispersion interactions are primarily responsible for the existence of the np form even without guest molecules.

A crucial test of our force field is its ability to also simulate the bistable behavior of the MIL-53(Al). Additionally, a force field is able to provide insight into the governing terms that lie on the origin of the breathing behavior. Therefore, we performed a scan that is representative for the breathing mode of MIL-53(Al) using the force field. The scan consists of a series of geometry optimizations in which we constrain the interdiagonal angle θ to values between 30° and 90° with steps of 1°, relaxing all other degrees of freedom during the geometry optimization. The procedure is similar to the one applied in section 3.6. To further investigate the importance of the vdW interactions, the scan procedure was repeated several times, but for each scan, another scale factor is used for the σ and/or ε parameters of the vdW expression (eq 6) relative to the tabulated MM3 values. The various energy profiles are displayed in Figure 7. Most curves show two minima, one at small interdiagonal angles that we can associate with the narrow pore phase (np) and one at higher interdiagonal angles that we can associate with the large pore phase (lp).

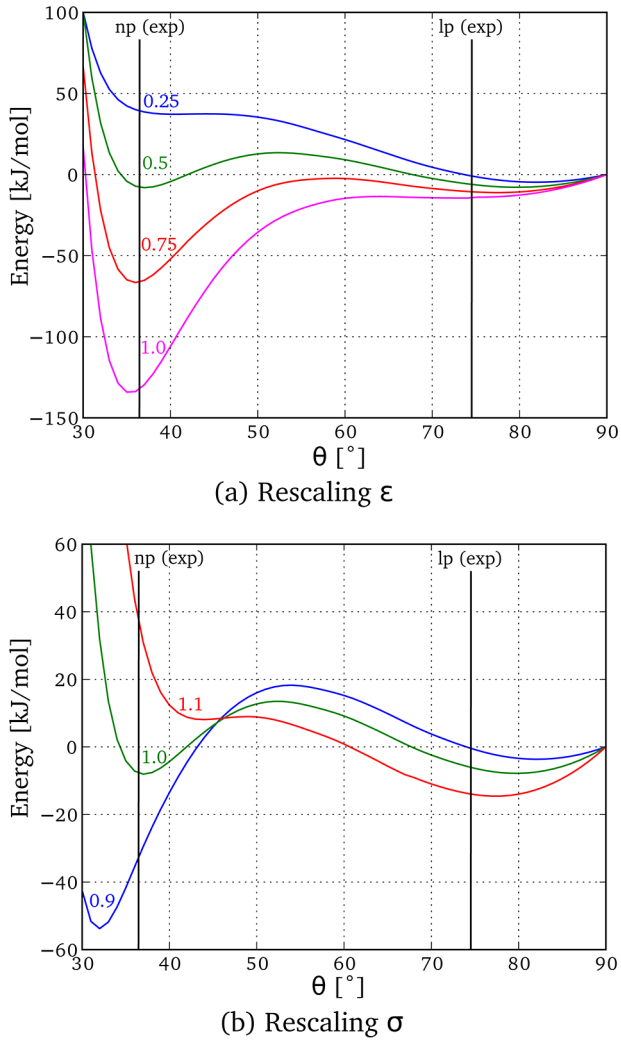

Figure 7. Energy profiles of the breathing mode for different sets of van der Waals parameters with indication of the interdiagonal angle of the experimental narrow pore and large pore phases.[31] (a) Total energy after uniformly rescaling the ε parameters of the vdW interactions and a σ scale factor of 1.0. (b) Total energy after uniformly rescaling the σ parameters and an ε scale factor of 0.5. The experimental values for the two local minima are taken from ref 28.

Without discussing the quantative features, this result is very promising, as apparently all curves indeed yield two minima. To further analyze the results, we first focus on the unscaled MM3 results in Figure 7a (scale factor = 1). We observe that the np is much more stable than the lp phase, by more than 60 kJ mol^{-1} per unit cell. This energy difference is too large compared to the result of Walker et al.[40] of 42 kJ mol^{-1}. The lp minimum is located around 74.3°, which is in good agreement with the experimental value of 73.7°,[28] but with an extremely low barrier. The interdiagonal angle of the np is predicted at 35.4°, also in good agreement with the experimental value of 36.5°.[28] In other words, the force-field simulation with unscaled MM3 parameters predicts two minima, lp and np, which are located at interdiagonal angles that are in very good agreement with the

dx.doi.org/10.1021/ct300172m | J. Chem. Theory Comput. 2012, 8, 3217−3231

experiment. However, the relative stability of the two minima does not agree with the results of Walker et al.

Next, we examine the sensitivity of the energy profile to the scaling factors of the van der Waals interactions. The upper figure (Figure 7a) displays the influence of decreasing the strength of the vdW interactions:

- The np becomes less stable, while its position remains unaffected.
- The position of the lp phase seems to shift slightly to larger interdiagonal angles, and its energy increases.

Rescaling the σ parameters induces other larger effects on the energy profile:

- The position of both the np and lp minimum are strongly dependent on the scale factor.
- Similar conclusions can be drawn for the stability of the two local minima. For a scale factor of 1.1, the relative stability is interchanged. The lp phase becomes more stable with respect to the np phase.

Another noteworthy feature is that also the shape of the unit cell is strongly dependent on the van der Waals interactions. This observation is confirmed by the current scan: varying both scales over the proposed range induces a variation in D of 0.4 Å and a variation in b of 0.16 Å in the large pore phase and even more in the narrow pore phase (see Table S4 in the Supporting Information).

Our tests with rescaled MM3-vdW parameters point out that it is crucial to have an accurate set of van der Waals parameters, in order to get a realistic energy profile of the breathing mode. The unscaled parameters of the MM3 force field are not entirely satisfactory as the relative stability of the two minima does not agree with Walker et al. Nevertheless, the two minima are present. Further model development is necessary to deduce more accurate forms for the van der Waals part of the force field. However, based on the results of Walker et al., we can propose a scale factor for the ε parameters that more accurately reproduces the relative stability. A linear interpolation between the results at ε scale factors 1.0 and 0.75 results in a scale factor of 0.86 with a corresponding relative stability of 42 kJ mol^{-1}.

5. CONCLUSIONS

A force field was developed for the metal organic framework MIL-53(Al) using density functional theory calculations on small nonperiodic clusters. Atomic partial charges, calculated using a Hirshfeld-I scheme on the valence molecular electron density, were used to calculate the electrostatic interactions of all atom pairs without any scaling, including 1−2, 1−3, and 1−4 pairs. The covalent parameters of the force field were fitted to reproduce the ab initio Hessian and forces using a least-squares cost function with two crucial adjustments that address mismatches in the geometry and strong correlations in the parameters. Two parameters figuring in the dihedral terms which contribute to the breathing behavior of the structure were refined using an ab initio scan in terms of the breathing angle using periodic DFT calculations. The van der Waals parameters of all atoms were taken from the MM3 force field.

The force field was validated for its ability to reproduce the geometry and cell parameters. The new force field predicts a geometry of the periodic MOF in its large pore form that closely matches the ab initio geometries of the core region in two well-chosen clusters, representative for the system of interest. The force field predicts unit cells of both the large pore and narrow pore phases with a shape that shows good agreement with the reported experimental data. Furthermore, the energy profile of the breathing mode was revealed to be highly dependent on the van der Waals parameters. The MM3 parameters succeed in reproducing a profile with two minima, although the np phase is predicted to be more stable than the theoretical data of Walker et al. By varying the van der Waals parameters, we showed that the energy profile can be tuned to predict also quantitatively the energies of the two phases more accurately.

In conclusion, the new force field was parametrized using a novel scheme for the covalent and electrostatic interactions and as such succeeds in predicting the geometries of the lp and np phases. However, to accurately describe the energy profile of the breathing mode, we need an improved set of van der Waals parameters. In the future, we plan to estimate van der Waals parameters specifically for MIL-53(Al) to overcome this deficiency. Additionally, future work is warranted to test the ability of the force field when also guest molecules are present in the material.

APPENDIX

We will now discuss in full detail how the parameters of the covalent interactions are estimated. Initially, the discussion is limited to a training set containing a single molecule. An extension with multiple molecules is trivial and will be discussed later. The calibration of the valence parameters is based on energy gradient and Hessian data derived from an ab initio computation on an isolated cluster that is representative for the system of interest. In practice, the geometry of the cluster is first optimized. However, we explicitly include the ab initio energy gradient in the equations to keep the derivation as general as possible.

Some conventions on the notation are systematically used below. The indices i and j are used for internal coordinates and runs from 1 to N_{ic}, the number of internal coordinates. μ and ν are indices used for Cartesian components and run from 1 to $3N_{at}$, with N_{at} being the total number of atoms. The potential energy is denoted by V, the gradient by G, and the Hessian by H. The model (force field or ab initio) in which this observable is calculated is specified in the superscript; e.g., V^{ff} represents the potential energy in the force field model. A contribution to these observables is specified in the subscript; e.g., V^{ff}_{cov} represents the covalent contribution to the potential energy in the force field model. Vector and matrix elements are denoted by means of brackets, e.g., $[G]_\mu$ and $[H]_{\mu\nu}$.

The most straightforward way to obtain valence parameters is to solve the following sets of equations:

$$G^{ai} = G^{ff}_{cov} + G^{ff}_{el} \tag{18}$$

$$H^{ai} = H^{ff}_{cov} + H^{ff}_{el} \tag{19}$$

where G^{ai}, G^{ff}_{cov}, and G^{ff}_{el} are $3N_{at} \times 1$ vectors containing the ab initio, covalent force-field, and electrostatic force-field gradients at the cluster geometry. Similarly, H^{ai}, H^{ff}_{cov}, and H^{ff}_{el} are the corresponding Hessian matrices with $3N_{at}$ by $3N_{at}$ second order derivatives. In these equations, only the covalent contributions depend on the valence parameters. The remaining contributions are constant matrices because the charges for the electrostatic term can be determined a priori. The total number of equations is in practice always larger than the number of parameters, certainly when information from multiple molecules is combined, which implies that the equations can only be

solved approximately using a least-squares procedure. Our experience is that these basic equations (with simple first and second order Cartesian derivatives of the energy) are not suitable for the calibration of valence parameters. Some crucial modifications are needed and discussed in the remainder of the Appendix.

A generic expression is used for the covalent force field to simplify the derivation:

$$V_{\mathrm{cov}}^{\mathrm{ff}} = \sum_{i}^{N_{\mathrm{ic}}} f_i(z_i, \alpha_{i1}, \alpha_{i2}, \ldots) \tag{20}$$

The sum runs over all internal coordinates, z_i, used in the force field model, e.g., bond lengths, bending angles, and dihedral angles. The internal coordinates, z_i, are known functions of $3N_{\mathrm{at}}$ Cartesian coordinates, x_μ. With each internal coordinate, an energy term, f_i, is associated, which contains a set of empirical parameters: α_{i1}, α_{i2}, and so on. These empirical parameters are calibrated to obtain an optimal correspondence between ab initio and force field data. The chain rule can be used to relate the Cartesian derivatives of the covalent energy in eqs 18 and 19 with derivatives of individual energy terms:

$$[G_{\mathrm{cov}}^{\mathrm{ff}}]_\mu = \frac{\partial V_{\mathrm{cov}}^{\mathrm{ff}}}{\partial x_\mu} = \sum_{i}^{N_{\mathrm{ic}}} \frac{\partial f_i(z_i, \alpha_{i1}, \alpha_{i2}, \ldots)}{\partial z_i} \frac{\partial z_i}{\partial x_\mu} \tag{21}$$

$$\begin{aligned}[H_{\mathrm{cov}}^{\mathrm{ff}}]_{\mu\nu} &= \frac{\partial V_{\mathrm{cov}}^{\mathrm{ff}}}{\partial x_\mu \partial x_\nu} \\ &= \sum_{i}^{N_{\mathrm{ic}}} \frac{\partial^2 f_i(z_i, \alpha_{i1}, \alpha_{i2}, \ldots)}{\partial z_i^2} \frac{\partial z_i}{\partial x_\mu} \frac{\partial z_i}{\partial x_\nu} \\ &\quad + \frac{\partial f_i(z_i, \alpha_{i1}, \alpha_{i2}, \ldots)}{\partial z_i} \frac{\partial^2 z_i}{\partial x_\mu \partial x_\nu}\end{aligned} \tag{22}$$

These equations can be written in matrix form as follows:

$$G_{\mathrm{cov}}^{\mathrm{ff}} = J\mathcal{G}_{\mathrm{cov}}^{\mathrm{ff}} \tag{23}$$

$$H_{\mathrm{cov}}^{\mathrm{ff}} = J\mathcal{H}_{\mathrm{cov}}^{\mathrm{ff}} J^T + \sum_{i}^{N_{\mathrm{ic}}} C_i [\mathcal{G}_{\mathrm{cov}}^{\mathrm{ff}}]_i \tag{24}$$

with

$$[J]_{\mu i} = \frac{\partial z_i}{\partial x_\mu} \tag{25}$$

$$[C_i]_{\mu\nu} = \frac{\partial^2 z_i}{\partial x_\mu \partial x_\nu} \tag{26}$$

$$[\mathcal{G}_{\mathrm{cov}}^{\mathrm{ff}}]_i = \frac{\partial f_i(z_i, \alpha_{i1}, \alpha_{i2}, \ldots)}{\partial z_i} \tag{27}$$

$$[\mathcal{H}_{\mathrm{cov}}^{\mathrm{ff}}]_{ij} = \delta_{ij} \frac{\partial^2 f_i(z_i, \alpha_{i1}, \alpha_{i2}, \ldots)}{\partial z_i^2} \tag{28}$$

The Jacobian, J, and the matrices, C_i, are constant during the calibration procedure. They depend on the molecular geometry and the choice of internal coordinates, which are fixed. All empirical parameters are found in the matrices with the first and second order derivatives of the energy terms, $\mathcal{G}_{\mathrm{cov}}^{\mathrm{ff}}$ and $\mathcal{H}_{\mathrm{cov}}^{\mathrm{ff}}$, respectively. Because each energy term only depends on one internal coordinate, the matrix $\mathcal{H}_{\mathrm{cov}}^{\mathrm{ff}}$ is diagonal. If cross terms would be present, it would also contain off-diagonal terms.

The two extensions discussed below are mainly related to the gradient equations (see eq 18), while the Hessian equations (see eq 19) are not modified. In both extensions, the Jacobian, J, plays a central role. In order to avoid any dependence on the choice of units for bond lengths and angles in the remainder of the Appendix, we rewrite equation eq 23 as follows:

$$G_{\mathrm{cov}}^{\mathrm{ff}} = \tilde{J} S \mathcal{G}_{\mathrm{cov}}^{\mathrm{ff}} \tag{29}$$

where S is a diagonal matrix with the norms of the columns of J and $\tilde{J}$ is a dimensionless matrix that contains the normalized columns of the Jacobian. Two matrices, which can be derived from $\tilde{J}$ with singular value decomposition (SVD), are used below: (i) a projection matrix P and (ii) an orthogonal complement $\tilde{J}_\perp$. The projection matrix P has orthonormal columns that form a basis for the columns of $\tilde{J}$. These basis vectors represent small changes in Cartesian coordinates that correspond to small changes in internal coordinates. It is not possible to write a small global translation or rotation as a linear combination of these basis vectors. The matrix $\tilde{J}_\perp$ has as rows an orthonormal basis for the orthogonal complement of the rows of $\tilde{J}$.

1. Transformed Gradient Equations

The first weakness of the gradient equations is that—when used in a least-squares context—the residual contribution is distributed equally over all components of the gradient, except for random fluctuations. In order to obtain parameters that accurately predict the molecular geometry, the gradient along shallow modes of the potential energy surface has to be more accurately determined than along modes with high curvature. This means that we have to introduce weights in the gradient equations to account for the variable sensitivity of the geometry to errors in the gradient. In order to give a higher weight to the gradient along shallow modes, one could multiply both sides of the gradient equations with the inverse of the ab initio Hessian.

$$(H^{\mathrm{ai}})^{-1} G^{\mathrm{ai}} = (H^{\mathrm{ai}})^{-1} (G_{\mathrm{cov}}^{\mathrm{ff}} + G_{\mathrm{el}}^{\mathrm{ff}}) \tag{30}$$

However, because the Hessian is a singular matrix, the inverse can only be defined in a subspace of the Cartesian coordinates. Therefore, we use the projection matrix P, which projects the Cartesian coordinates to the subspace of the internal coordinates. The final transformed gradient equations become:

$$(PH^{\mathrm{ai}}P^T)^{-1} PG^{\mathrm{ai}} = (PH^{\mathrm{ai}}P^T)^{-1} P(G_{\mathrm{cov}}^{\mathrm{ff}} + G_{\mathrm{el}}^{\mathrm{ff}}) \tag{31}$$

One could also interpret this transformation as a single step from the Newton optimization algorithm. In practice, one uses ab initio optimized geometries for the parameter calibration, which implies that the left-hand side is zero. The right-hand side is then an approximate error on the force-field geometry in a coordinate space that excludes global rotation and translation. Hence, these equations impose a good force-field geometry without having to perform the actual geometry optimization during the calibration procedure. In principle, one could also use the force-field Hessian on the right-hand side of eq 31, but this would introduce a strong nonlinear dependence of the equations in the parameters, leading to a much harder nonlinear least-squares problem.

2. Internal Strain Equations

A second weakness of the gradient equations is that the Jacobian in eq 23 transforms the vector with derivatives of energy terms to a lower dimensional space to obtain the

Cartesian energy derivatives. It is therefore unavoidable that the Cartesian gradient of the covalent energy becomes insensitive to some linear combinations of derivatives of energy terms. The simplest example can be found in cyclopropane, where it is impossible to increase or reduce the three C−C−C angles simultaneously. If a cyclopropane force field would have a C−C−C rest-angle different from 60°, the equilibrium angle would still be 60°. We will denote such internal forces that cancel each other out as *internal strain*. In the case of cyclopropane, it is impossible to determine the value of the C−C−C rest angle from Cartesian training data. One has two options to solve this type of problem: (i) introduce constraints to fix such parameters or (ii) introduce additional equations in the least-squares fit to fix these parameters. We propose a solution in line with the second option.

One can quantify the amount of internal strain using the orthogonal complement $\tilde{J}_\perp$ as follows:

$$Y^{\mathrm{ff}}_{\mathrm{cov}} = \tilde{J}_\perp S \mathcal{G}^{\mathrm{ff}}_{\mathrm{cov}} \tag{32}$$

A new symbol, $Y^{\mathrm{ff}}_{\mathrm{cov}}$, is used to stress that the internal strain is complementary to the Cartesian gradient. All the degrees of freedom that are discarded (projected out) when computing the Cartesian gradient of the covalent energy are present in $Y^{\mathrm{ff}}_{\mathrm{cov}}$. The additional least-squares equations are obtained by simply requiring that the internal strains are equal to zero:

$$Y^{\mathrm{ff}}_{\mathrm{cov}} = 0 \tag{33}$$

In the example of cyclopropane, such equations force the rest value parameter to be 60°. Also in more complex cases, these equations impose realistic values for the rest parameters.

3. Total Cost Function

So far, three sets of least squares equations are defined, all having different units: transformed gradient (tg) equations in Å, Hessian (h) equations in kJ mol^{-1} Å^{-2}, and internal strain (is) equations in kJ mol^{-1} Å^{-1}. For each set of equations, we write the difference between the left-hand and right-hand side of the kth equation as $\mathrm{Err}^{\mathrm{XX}}_k$ where XX is tg, h, or is. One can find a set of covalent force-field parameters that approximately solves all equations by minimizing a total cost function:

$$X = \frac{1}{\sigma^2_{\mathrm{tg}} N_{\mathrm{tg}}} \sum_{k=1}^{N_{\mathrm{tg}}} (\mathrm{Err}^{\mathrm{tg}}_k)^2 + \frac{1}{\sigma^2_{\mathrm{h}} N_{\mathrm{h}}} \sum_{k=1}^{N_{\mathrm{h}}} (\mathrm{Err}^{\mathrm{h}}_k)^2 + \frac{1}{\sigma^2_{\mathrm{is}} N_{\mathrm{is}}} \sum_{k=1}^{N_{\mathrm{is}}} (\mathrm{Err}^{\mathrm{is}}_k)^2 \tag{34}$$

where the *scales* (σ_{tg}, σ_{h}, and σ_{is}) have the same unit as the corresponding equations. They must be tuned to obtain a well-defined least-squares problem. We could not find universal values for these scales. We experience that a good choice for the scales depends on the system for which a force field is being developed. There are two criteria that can be used as a guidance to tune the scales: (i) one should obtain a condition number for the least squares fit that is as low as possible, and (ii) the scales should roughly correspond to acceptable orders of magnitude for the root-mean-square errors on each set of equations. (The condition number is defined as the ratio of the highest and lowest eigenvalue of the Hessian of the cost function at the optimal parameters.)

When one uses a training set with multiple molecules for the force-field calibration, one can simply minimize the sum of the corresponding cost functions. For the calibration of the MIL-53(Al) force field, only the core regions were used from two clusters. Equations that are not related to the atoms in the core region were omitted from the cost function. Because the force field contains nonlinear parameters, one should carefully choose reasonable initial values prior to the calibration procedure.

■ ASSOCIATED CONTENT

Supporting Information

The following additional information is included: an unused deficient oxide cluster, the atomic coordinates and Hirshfeld-based charges of the DFT-optimized clusters, the cell dimensions as a function of the van der Waals scale factors, and a sensitivity analysis of D and θ toward K_c and K_o. This material is available free of charge via the Internet at http://pubs.acs.org/.

■ AUTHOR INFORMATION

Corresponding Author

*E-mail: Toon.Verstraelen@Ugent.be; Veronique.VanSpeybroeck@Ugent.be.

Notes

The authors declare no competing financial interest.

■ ACKNOWLEDGMENTS

This work is supported by the Fund for Scientific Research; Flanders (FWO), the Research Board of Ghent University (BOF) and BELSPO in the frame of IAP/6/27. Funding was also received from the European Research Council under the European Community's Seventh Framework Programme [FP7(2007-2013) ERC grant agreement number 240483]. Computational resources (Stevin Supercomputer Infrastructure) and services were provided by Ghent University.

■ REFERENCES

(1) Li, H.; Eddaoudi, M.; O'Keeffe, M.; Yaghi, O. *Nature* **1999**, *402*, 276−279.
(2) Eddaoudi, M.; Kim, J.; Rosi, N.; Vodak, D.; Wachter, J.; O'Keeffe, M.; Yaghi, O. *Science* **2002**, *295*, 469−472.
(3) Long, J.; Yaghi, O. *Chem. Soc. Rev.* **2009**, *38*, 1213−1214.
(4) Kitagawa, S.; Noro, S.-I.; Kitaura, R. *Angew. Chem., Int. Ed.* **2004**, *43*, 2334−2375.
(5) Kitagawa, S.; Noro, S.-I.; Nakamura, T. *Chem. Commun.* **2006**, 701−707.
(6) Trung, T.; Trens, P.; Tanchoux, N.; Bourrelly, S.; Llewellyn, P.; Loera-Serna, S.; Serre, C.; Loiseau, T.; Fajula, F.; Férey, G. *J. Am. Chem. Soc.* **2008**, *130*, 16926−16932.
(7) Férey, G. *Chem. Soc. Rev.* **2008**, *37*, 191−214.
(8) Perry, J.; Perman, J.; Zaworotko, M. *Chem. Soc. Rev.* **2009**, *38*, 1400−1417.
(9) Tranchemontagne, D. J.; Mendoza-Cortes, J. L.; O'Keeffe, M.; Yaghi, O. *Chem. Soc. Rev.* **2009**, *38*, 1257−1283.
(10) Meek, S.; Greathouse, J.; Allendorf, M. *Adv. Mater.* **2011**, *23*, 249−267.
(11) Deng, H.; Grunder, S.; Cordova, K. E.; Valente, C.; Furukawa, H.; Hmadeh, M.; Gándara, F.; Whalley, A. C.; Liu, Z.; Asahina, S.; Kazumori, H.; O'Keeffe, M.; Terasaki, O.; Stoddart, J. F.; Yaghi, O. M. *Science* **2012**, *336*, 1018−1023.
(12) Furukawa, H.; Ko, N.; Go, Y. B.; Aratani, N.; Choi, S. B.; Choi, E.; Yazaydin, A. O.; Snurr, R. Q.; O'Keeffe, M.; Kim, J.; Yaghi, O. M. *Science* **2010**, *329*, 424−428.
(13) Mulder, F.; Dingemans, T.; Schimmel, H.; Ramirez-Cuesta, A.; Kearley, G. *Chem. Phys.* **2008**, *351*, 72−76.
(14) Himsl, D.; Wallacher, D.; Hartmann, M. *Angew. Chem., Int. Ed.* **2009**, *48*, 4639−4642.

(15) Bourrelly, S.; Llewellyn, P.; Serre, C.; Millange, F.; Loiseau, T.; Férey, G. *J. Am. Chem. Soc.* **2005**, *127*, 13519−13521.
(16) Millward, A.; Yaghi, O. *J. Am. Chem. Soc.* **2005**, *127*, 17998−17999.
(17) Li, Y.; Yang, R. *Langmuir* **2007**, *23*, 12937−12944.
(18) Couck, S.; Denayer, J.; Baron, G.; Remy, T.; Gascon, J.; Kapteijn, F. *J. Am. Chem. Soc.* **2009**, *131*, 6326−6327.
(19) D'Alessandro, D.; Smit, B.; Long, J. *Angew. Chem., Int. Ed.* **2010**, *49*, 6058−6082.
(20) Férey, G.; Serre, C.; Devic, T.; Maurin, G.; Jobic, H.; Llewellyn, P.; De Weireld, G.; Vimont, A.; Daturi, M.; Chang, J. *Chem. Soc. Rev.* **2011**, *40*, 550−562.
(21) Alaerts, L.; Kirschhock, C.; Maes, M.; van der Veen, M.; Finsy, V.; Depla, A.; Martens, J.; Baron, G.; Jacobs, P.; Denayer, J.; De Vos, D. *Angew. Chem., Int. Ed.* **2007**, *46*, 4293−4297.
(22) Alaerts, L.; Maes, M.; Giebeler, L.; Jacobs, P.; Martens, J.; Denayer, J.; Kirschhock, C.; De Vos, D. *J. Am. Chem. Soc.* **2008**, *130*, 14170−14178.
(23) Leus, K.; Muylaert, I.; Vandichel, M.; Marin, G.; Waroquier, M.; Van Speybroeck, V.; Van der Voort, P. *Chem. Commun.* **2010**, *46*, 5085−5087.
(24) Leus, K.; Vandichel, M.; Liu, Y.-Y.; Muylaert, I.; Musschoot, J.; Pyl, S.; Vrielinck, H.; Callens, F.; Marin, G.; Detavernier, C.; Wiper, P.; Khimyak, Y.; Waroquier, M.; Van Speybroeck, V.; Van der Voort, P. *J. Catal.* **2012**, *285*, 196−207.
(25) Vermoortele, F.; Vandichel, M.; Van de Voorde, B.; Ameloot, R.; Waroquier, M.; Van Speybroeck, V.; De Vos, D. E. *Angew. Chem., Int. Ed.* **2012**, *51*, 4887−4890.
(26) Corma, A.; García, H.; Llabrés i Xamena, F. X. *Chem. Rev.* **2010**, *110*, 4606−4655.
(27) Farrusseng, D.; Aguado, S.; Pinel, C. *Angew. Chem., Int. Ed.* **2009**, *48*, 7502−7513.
(28) Liu, Y.; Her, J.; Dailly, A.; Ramirez-Cuesta, A.; Neumann, D.; Brown, C. *J. Am. Chem. Soc.* **2008**, *130*, 11813−11818.
(29) Beurroies, I.; Boulhout, M.; Llewellyn, P. L.; Kuchta, B.; Férey, G.; Serre, C.; Denoyel, R. *Angew. Chem., Int. Ed.* **2010**, *49*, 7526−7529.
(30) Murray, K.; Kepert, C. *Top. Curr. Chem.* **2004**, *233*, 195−228.
(31) Loiseau, T.; Serre, C.; Huguenard, C.; Fink, G.; Taulelle, F.; Henry, M.; Bataille, T.; Férey, G. *Chem.—Eur. J.* **2004**, *10*, 1373−1382.
(32) Llewellyn, P.; Bourrelly, S.; Serre, C.; Filinchuk, Y.; Férey, G. *Angew. Chem., Int. Ed.* **2006**, *45*, 7751−7754.
(33) Serre, C.; Millange, F.; Thouvenot, C.; Noguès, M.; Marsolier, G.; Louër, D.; Férey, G. *J. Am. Chem. Soc.* **2002**, *124*, 13519−13526.
(34) Serre, C.; Mellot-Draznieks, C.; Surblé, S.; Audebrand, N.; Filinchuk, Y.; Férey, G. *Science* **2007**, *315*, 1828−1831.
(35) Anokhina, E. V.; Vougo-Zanda, M.; Wang, X.; Jacobson, A. J. *J. Am. Chem. Soc.* **2005**, *127*, 15000−15001.
(36) Whitfield, T. R.; Wang, X.; Liu, L.; Jacobson, A. J. *Solid State Sci.* **2005**, *7*, 1096−1103.
(37) Vougo-Zanda, M.; Huang, J.; Anokhina, E.; Wang, X.; Jacobson, A. J. *Inorg. Chem.* **2008**, *47*, 11535−11542.
(38) Bauer, S.; Serre, C.; Devic, T.; Horcajada, P.; Marrot, J.; Férey, G.; Stock, N. *Inorg. Chem.* **2008**, *47*, 7568−7576.
(39) Mowat, J. P.; Miller, S. R.; Slawin, A. M.; Seymour, V. R.; Ashbrook, S. E.; Wright, P. A. *Microporous Mesoporous Mater.* **2011**, *142*, 322−333.
(40) Walker, A.; Civalleri, B.; Slater, B.; Mellot-Draznieks, C.; Corà, F.; Zicovich-Wilson, C.; Román-Pérez, G.; Soler, J.; Gale, J. *Angew. Chem., Int. Ed.* **2010**, *49*, 7501−7503.
(41) Smit, B.; Maesen, T. L. M. *Chem. Rev.* **2008**, *108*, 4125−4184.
(42) Walton, K. S.; Millward, A. R.; Dubbeldam, D.; Frost, H.; Low, J. J.; Yaghi, O. M.; Snurr, R. Q. *J. Am. Chem. Soc.* **2008**, *130*, 406−407.
(43) Dubbeldam, D.; Krishna, R.; Snurr, R. Q. *J. Phys. Chem. C* **2009**, *113*, 19317−19327.
(44) Duren, T.; Bae, Y.-S.; Snurr, R. Q. *Chem. Soc. Rev.* **2009**, *38*, 1237−1247.
(45) Grimme, S. *J. Comput. Chem.* **2006**, *27*, 1787−1799.
(46) Grimme, S.; Antony, J.; Ehrlich, S.; Krieg, H. *J. Chem. Phys.* **2010**, *132*, 154104.
(47) Zhao, Y.; Truhlar, D. *Theor. Chem. Acc.* **2008**, *120*, 215−241.
(48) Zhao, Y.; Truhlar, D. *Acc. Chem. Res.* **2008**, *41*, 157−167.
(49) Chai, J.-D.; Head-Gordon, M. *Phys. Chem. Chem. Phys.* **2008**, *10*, 6615−6620.
(50) Dion, M.; Rydberg, H.; Schröder, E.; Langreth, D.; Lundqvist, B. *Phys. Rev. Lett.* **2004**, *92*, 246401−246404.
(51) Lee, K.; Murray, E. D.; Kong, L.; Lundqvist, B. I.; Langreth, D. C. *Phys. Rev. B* **2010**, *82*, 081101−081104.
(52) Poloni, R.; Smit, B.; Neaton, J. *J. Phys. Chem. A* **2012**, *116*, 4957−4964.
(53) Rappé, A.; Casewit, C.; Colwell, K.; Goddard, W.; Skiff, W. *J. Am. Chem. Soc.* **1992**, *114*, 10024−10035.
(54) Mayo, S.; Olafson, B.; Goddard, W. *J. Phys. Chem.* **1990**, *94*, 8897−8909.
(55) Dauber-Osguthorpe, P.; Roberts, V.; Osguthorpe, D.; Wolff, J.; Genest, M.; Hagler, A. *Proteins: Struct., Funct., Genet.* **1988**, *4*, 31−47.
(56) Allinger, N.; Lii, J.; Yuh, Y. *J. Am. Chem. Soc.* **1989**, *111*, 8551−8566.
(57) Salles, F.; Ghoufi, A.; Maurin, G.; Bell, R.; Mellot-Draznieks, C.; Férey, G. *Angew. Chem., Int. Ed.* **2008**, *47*, 8487−8491.
(58) Tafipolsky, M.; Amirjalayer, S.; Schmid, R. *J. Comput. Chem.* **2007**, *28*, 1169−1175.
(59) Tafipolsky, M.; Schmid, R. *J. Phys. Chem. B* **2009**, *113*, 1341−1352.
(60) Tafipolsky, M.; Amirjalayer, S.; Schmid, R. *J. Phys. Chem. C* **2010**, *114*, 14402−14409.
(61) Tafipolsky, M.; Amirjalayer, S.; Schmid, R. *Angew. Chem., Int. Ed.* **2007**, *46*, 463−466.
(62) Dubbeldam, D.; Walton, K. S.; Ellis, D. E.; Snurr, R. Q. *Angew. Chem., Int. Ed.* **2007**, *46*, 4496−4499.
(63) Ford, D. C.; Dubbeldam, D.; Snurr, R. Q.; Künzel, V.; Wehring, M.; Stallmach, F.; Kärger, J.; Müller, U. *J. Phys. Chem. Lett.* **2012**, *3*, 930−933.
(64) Becke, A. *Phys. Rev. A* **1988**, *38*, 3098.
(65) Becke, A. *J. Chem. Phys.* **1993**, *98*, 5648−5652.
(66) Lee, C.; Yang, W.; Parr, R. *Phys. Rev. B* **1988**, *37*, 785.
(67) Zygmunt, S.; Mueller, R.; Curtiss, L.; Iton, L. *THEOCHEM* **1998**, *430*, 9−16.
(68) Sousa, S.; Fernandes, P.; Ramos, M. *J. Phys. Chem. A* **2007**, *111*, 10439−10452.
(69) Krishnan, R.; Binkley, J. S.; Seeger, R.; Pople, J. A. *J. Chem. Phys.* **1980**, *72*, 650−654.
(70) McLean, A. D.; Chandler, G. S. *J. Chem. Phys.* **1980**, *72*, 5639−5648.
(71) Frisch, M. J.; Pople, J. A.; Binkley, J. S. *J. Chem. Phys.* **1984**, *80*, 3265−3269.
(72) Ditchfield, R.; Hehre, W. J.; Pople, J. A. *J. Chem. Phys.* **1971**, *54*, 724−728.
(73) Frisch, M.; Trucks, G.; Schlegel, H.; Scuseria, G.; Robb, M.; Cheeseman, J.; Scalmani, G.; Barone, V.; Mennucci, B.; Petersson, G.; Nakatsuji, H.; Caricato, M.; Li, X.; Hratchian, H.; Izmaylov, A.; Bloino, J.; Zheng, G.; Sonnenberg, J.; Hada, M.; Ehara, M.; Toyota, K.; Fukuda, R.; Hasegawa, J.; Ishida, M.; Nakajima, T.; Honda, Y.; Kitao, O.; Nakai, H.; Vreven, T.; Montgomery, J.; Peralta, J.; Ogliaro, F.; Bearpark, M.; Heyd, J.; Brothers, E.; Kudin, K.; Staroverov, V.; Kobayashi, R.; Normand, J.; Raghavachari, K.; Rendell, A.; Burant, J.; Iyengar, S.; Tomasi, J.; Cossi, M.; Rega, N.; Millam, J.; Klene, M.; Knox, J.; Cross, J.; Bakken, V.; Adamo, C.; Jaramillo, J.; Gomperts, R.; Stratmann, R.; Yazyev, O.; Austin, A.; Cammi, R.; Pomelli, C.; Ochterski, J.; Martin, R.; Morokuma, K.; Zakrzewski, V.; Voth, G.; Salvador, P.; Dannenberg, J.; Dapprich, S.; Daniels, A.; Farkas, O.; Foresman, J.; Ortiz, J.; Cioslowski, J.; Fox, D. *Gaussian 09*, revision A.02; Gaussian Inc.: Wallingford, CT, 2009.
(74) Perdew, J.; Burke, K.; Ernzerhof, M. *Phys. Rev. Lett.* **1996**, *77*, 3865−3868.
(75) Perdew, J.; Burke, K.; Ernzerhof, M. *Phys. Rev. Lett.* **1997**, *78*, 1396−1396.

(76) Mortensen, J.; Hansen, L.; Jacobsen, K. *Phys. Rev. B* **2005**, *71*, 035109−035119.
(77) Enkovaara, J.; Rostgaard, C.; Mortensen, J.; Chen, J.; Dułak, M.; Ferrighi, L.; Gavnholt, J.; Glinsvad, C.; Haikola, V.; Hansen, H.; Kristoffersen, H.; Kuisma, M.; Larsen, A.; Lehtovaara, L.; Ljungberg, M.; Lopez-Acevedo, O.; Moses, P.; Ojanen, J.; Olsen, T.; Petzold, V.; Romero, N.; Stausholm-Møller, J.; Strange, M.; Tritsaris, G.; Vanin, M.; Walter, M.; Hammer, B.; Häkkinen, H.; Madsen, G.; Nieminen, R.; Nørskov, J.; Puska, M.; Rantala, T.; Schiøtz, J.; Thygesen, K.; Jacobsen, K. *J. Phys.: Condens. Matter* **2010**, *22*, 253202−253225.
(78) Bahn, S.; Jacobsen, K. *Comput. Sci. Eng.* **2002**, *4*, 56−66.
(79) Blöchl, P. E. *Phys. Rev. B* **1994**, *50*, 17953−17979.
(80) Blöchl, P. E.; Först, C. J.; Schimpl, J. *Bull. Mater. Sci.* **2003**, *26*, 33−41.
(81) Kresse, G.; Furthmuller, J. *Comput. Mater. Sci.* **1996**, *6*, 15−50.
(82) Hafner, J. *J. Comput. Chem.* **2008**, *29*, 2044−2078.
(83) Kresse, G.; Joubert, D. *Phys. Rev. B* **1999**, *59*, 1758.
(84) Ewald, P. P. *Ann. Phys.* **1921**, *369*, 253−287.
(85) De Moor, B.; Ghysels, A.; Reyniers, M.; Van Speybroeck, V.; Waroquier, M.; Marin, G. *J. Chem. Theory Comput.* **2011**, *7*, 1090−1101.
(86) Verstraelen, T.; Van Speybroeck, V.; Waroquier, M. *J. Chem. Inf. Model.* **2008**, *48*, 1530−1541.
(87) Allured, V.; Kelly, C.; Landis, C. *J. Am. Chem. Soc.* **1991**, *113*, 1.
(88) Rappe, A.; Bormann-Rochotte, L.; Wiser, D.; Hart, J.; Pietsch, M.; Casewit, C.; Skiff, W. *Mol. Phys.* **2007**, *105*, 301.
(89) Mulliken, R. S. *J. Chem. Phys.* **1955**, *23*, 1833−1840.
(90) Reed, A. E.; Weinstock, R. B.; Weinhold, F. *J. Chem. Phys.* **1985**, *83*, 735−746.
(91) Hirshfeld, F. *Theor. Chim. Acta* **1977**, *44*, 129.
(92) Bultinck, P.; Van Alsenoy, C.; Ayers, P. W.; Carbo-Dorca, R. *J. Chem. Phys.* **2007**, *126*, 144111.
(93) Singh, U. C.; Kollman, P. A. *J. Comput. Chem.* **1984**, *5*, 129−145.
(94) Breneman, C. M.; Wiberg, K. B. *J. Comput. Chem.* **1990**, *11*, 361−373.
(95) Bayly, C.; Cieplak, P.; Cornell, W.; Kollman, P. *J. Phys. Chem.* **1993**, *97*, 10269−10280.
(96) Bader, R. F. W. *Chem. Rev.* **1991**, *91*, 893−928.
(97) Bush, B. L.; Bayly, C. I.; Halgren, T. A. *J. Comput. Chem.* **1999**, *20*, 1495−1516.
(98) Ponder, J. W.; Case, D. A. *Adv. Protein Chem.* **2003**, *66*, 27−85.
(99) Ramsahye, N.; Maurin, G.; Bourrelly, S.; Llewellyn, P.; Férey, G. *Phys. Chem. Chem. Phys.* **2007**, *9*, 1059−1063.
(100) Verstraelen, T.; Pauwels, E.; De Proft, F.; Van Speybroeck, V.; Geerlings, P.; Waroquier, M. *J. Chem. Theory Comput.* **2012**, *8*, 661−676.
(101) Press, W. H.; Teukolsky, S. A.; Vetterling, W. T.; Flannery, B. P. *Numerical Recipes: The Art of Scientific Computing*, 3rd ed.; Cambridge University Press: New York, NY, 2007; Chapter Solution of Linear Algebraic Equations, pp 65−75.
(102) Halgren, T. A. *J. Comput. Chem.* **1996**, *17*, 520−552.
(103) Van Damme, S.; Bultinck, P.; Fias, S. *J. Chem. Theory Comput.* **2009**, 334−340.
(104) Catak, S.; D'hooghe, M.; Verstraelen, T.; Hemelsoet, K.; Van Nieuwenhove, A.; Ha, H.-J.; Waroquier, M.; De Kimpe, N.; Van Speybroeck, V. *J. Org. Chem.* **2010**, *75*, 4530−4541.
(105) Verstraelen, T.; Sukhomlinov, S. V.; Van Speybroeck, V.; Waroquier, M.; Smirnov, K. S. *J. Phys. Chem. C* **2012**, *116*, 490−504.
(106) Allinger, N. L.; Zhou, X.; Bergsma, J. *THEOCHEM* **1994**, *312*, 69−83.
(107) Ponder, J. W. *TINKER − Software Tools for Molecular Design*; Washington University in Saint Louis: Saint Louis, MO, 2011. http://dasher.wustl.edu/ffe/ (accessed on January 11, 2012).
(108) Ercolessi, F.; Adams, J. B. *Europhys. Lett.* **1994**, *26*, 583−588.
(109) Xie, T.; Bowman, J. M. *J. Chem. Phys.* **2002**, *117*, 10487−10492.
(110) Carbonniere, P.; Begue, D.; Dargelos, A.; Pouchan, C. *Chem. Phys.* **2004**, *300*, 41−51.
(111) Verstraelen, T.; Van Neck, D.; Ayers, P. W.; Van Speybroeck, V.; Waroquier, M. *J. Chem. Theory Comput.* **2007**, *3*, 1420−1434.
(112) Sparta, M.; Hansen, M. B.; Matito, E.; Toffoli, D.; Christiansen, O. *J. Chem. Theory Comput.* **2010**, *6*, 3162−3175.
(113) van Duin, A. C. T.; Dasgupta, S.; Lorant, F.; Goddard, W. A. *J. Phys. Chem. A* **2001**, *105*, 9396−9409.
(114) Martin, M. G.; Siepmann, J. I. *J. Phys. Chem. B* **1998**, *102*, 2569−2577.
(115) Liu, B.; Smit, B.; Rey, F.; Valencia, S.; Calero, S. *J. Phys. Chem. C* **2008**, *112*, 2492−2498.
(116) Maerzke, K. A.; Siepmann, J. I. *J. Phys. Chem. B* **2011**, *115*, 3452−3465.
(117) Hill, J.-R.; Sauer, J. *J. Phys. Chem.* **1995**, *99*, 9536−9550.
(118) CMM Software. http://molmod.ugent.be/software (accessed on July 24, 2012).
(119) Chai, J.-D.; Head-Gordon, M. *J. Chem. Phys.* **2008**, *128*, 084106.